ORIENTATION-DEPENDENT ACOUSTIC BEHAVIOUR OF FOAM-FORMED REED AND LUPINE FIBRE ABSORBERS: LIMITATIONS OF HOMOGENEOUS POROUS MODELLING

Janis Heldmann[1], Marike Langhans[2], Tapio Lokki[1]

[1] *Department of Information & Communication Engineering, School of Electrical Engineering, Aalto University, Espoo, Finland*

[2] *Department of Chemistry & Material Science, School of Chemical Engineering, Aalto University, Espoo, Finland*

This paper is a revised version of the authors' submitted manuscript that was peer-reviewed by at least two anonymous reviewers.

Abstract

Foam-formed plant fibre materials are promising sustainable sound absorbers, but their manufacture creates dense drainage layers, producing internal density gradients that violate the homogeneity assumption of standard equivalent-fluid models such as the Johnson–Champoux–Allard–Lafarge (JCAL) model. We investigate foam-formed reed and lupine fibre materials using impedance tube measurements from both the open surface (Side A) and the drainage-mesh surface (Side B). The measured absorption depends clearly on orientation: with the dense layer near the rigid backing (Side A), JCAL inversion and analytical fibrous models reproduce the absorption well, whereas with it facing the source (Side B), the enhanced low-frequency performance cannot be captured by homogeneous modelling. Model parameters obtained by inverse characterisation are therefore configuration-dependent rather than intrinsic. Standard airflow resistivity measurements are further shown to be dominated by the thin drainage layer. These results establish Side A characterisation as the appropriate basis for deriving intrinsic fibre parameters in inhomogeneous foam-formed materials.

Keywords: *porous materials, fibrous absorbers, acoustic modelling, foam forming, bio-based acoustics, layered materials*

1. Introduction

Sustainable acoustic materials based on plant fibres are attracting increasing attention as alternatives to conventional mineral or polymeric sound absorbers [1]. Foam forming has emerged as a promising manufacturing process for such materials, enabling the production of lightweight porous structures with high porosity [2], [3]. The acoustic potential of foam-formed materials has been demonstrated for softwood fibres [4], [5] and more recently for reed and lupine fibres [3], with absorption performance comparable to conventional fibrous absorbers.

A key challenge in modelling foam-formed materials is their inherent microstructural inhomogeneity. During foam forming, gravitational drainage causes fibres to sediment toward the bottom of the mould, creating a denser and more compact layer at the drainage mesh surface. This density gradient violates the homogeneity assumption underlying standard equivalent fluid models such as the JCAL model [6], which require a single set of non-acoustic parameters to describe the entire material.

Previous work on foam-formed softwood fibres addressed this by physically removing the dense drainage layer before measurement, ensuring that the remaining sample was sufficiently homogeneous for JCAL characterisation [4]. However, this approach discards a structurally and acoustically significant part of the material. The present work takes a different approach: the reed and lupine samples are measured intact, from both orientations, in order to directly expose the consequences of the density gradient for acoustic measurement and modelling.

The aim of this work is twofold. First, to demonstrate experimentally that the acoustic response of foam-formed plant fibre materials depends on sample orientation and to quantify the failure of homogeneous JCAL models in the orientation where the dense layer dominates. Second, to establish a physically grounded approach to analytical modelling that uses only orientation-independent material parameters derived from the more reliable Side A characterisation.

Corresponding author: *janis.heldmann@aalto.fi.*

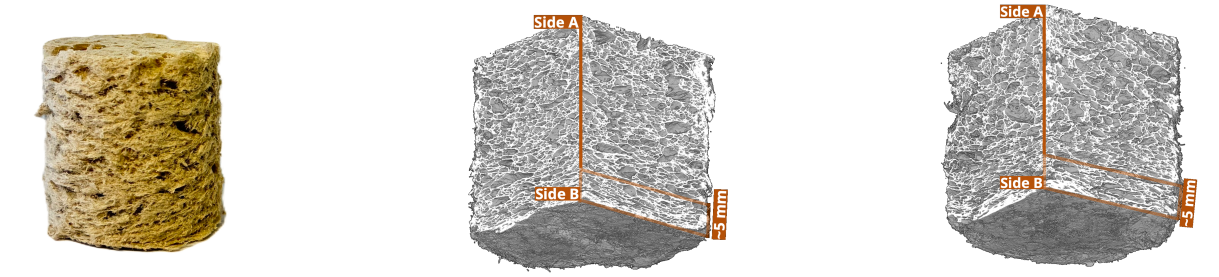

(a) Foam-formed sample. **(b)** Reed, X-ray tomography. **(c)** Lupine, X-ray tomography.

Figure 1: (a) Photograph of a foam-formed fibre sample cut to impedance tube diameter. (b, c) Reconstructed 3D images of X-ray tomography scans from reed and lupine samples, shown with the open surface (Side A) uppermost and the drainage-mesh surface (Side B) at the bottom. In both materials the fibre network is open and highly porous through most of the thickness, while a visibly denser, compacted layer of approximately 5 mm extends upward from the drainage surface [3]. This layer is the structural origin of the orientation-dependent absorption reported in Section 5.

2. Materials and Experimental Data

The materials investigated are foam-formed samples produced from reed (*Phragmites australis*) and lupine (*Lupinus polyphyllus*) fibres. The latter is invasive in Finland and represents an underutilised lignocellulosic resource. The fibres were soda-pulped and foam-formed at three fibre consistencies, producing three bulk density levels per material in the range of approximately 24 to 36 $\mathrm{kg\,m^{-3}}$, with porosities exceeding 0.97. Four samples were produced per fibre consistency; the reported bulk densities are medians across these four samples, and the absorption coefficients are averages over them. Full details of the pulping and foam-forming are reported elsewhere [3].

Whole-sample airflow resistivity was measured following ISO 9053 [3]. As is shown in Section 5, these measurements are dominated by the dense drainage layer and are not representative of the bulk material.

Normal-incidence sound absorption coefficients were measured using an impedance tube with a three-microphone transfer function method [7], [8] over the frequency range 250 to 6300 Hz. Each sample was measured from both sides. Side A denotes the open top surface, which is representative of the relatively homogeneous bulk fibre network. Side B denotes the bottom surface formed against the drainage mesh, which features a denser and more compact layer due to gravitational drainage during foam forming. This is the opposite convention to the softwood study [4], where the drainage layer was removed entirely: here it is retained and its acoustic consequences are the primary object of investigation.

Figure 1 shows a foam-formed sample together with reconstructed 3 dimensional X-ray tomographs of reed and lupine, in which the density gradient is directly visible: an open fibre network occupies most of the sample thickness, while a compacted layer of approximately 5 mm is present at the drainage surface in both materials.

3. Analytical Modelling

The analytical fibrous medium model introduced in [4] is used to predict the JCAL non-acoustic parameters from the fibre radius and porosity. The porosity ϕ is computed from bulk density ρ and fibre density $\rho_f = 1500\,\mathrm{kg\,m^{-3}}$ as

$$\phi = 1 - \frac{\rho}{\rho_f}.$$

The airflow resistivity is predicted using a modified Tamayol relation [9] accounting for fibre overlap and random orientation [10]. The tortuosity is estimated from an Archie-type relation [11], and the viscous and thermal characteristic lengths from analytical expressions for parallel fibre arrays [12]. Due to limitation of the parallel fibre model for randomly-distributed fibre networks the expression for the viscous characteristic length has been replaced with an exponential correlation according to [4].

The effective fibre radius a_{eff} and density are the key input parameters. The whole-sample measured flow resistivity cannot be used to derive a_{eff}: as demonstrated in Section 5, it is dominated by the thin dense drainage layer and overestimates the bulk resistivity by a large factor. Instead, a_{eff} is derived from the JCAL-characterised Side A values, which are representative of the bulk fibre network. Because the modified Tamayol relation depends on the radius only through a $1/a^2$ prefactor for fixed literature coefficients ($c_1 = 0.21$, $c_2 = 0.71$), the resistivity relation is inverted analytically at each density and the resulting radii are averaged, treating a_{eff} as a density-independent material constant; their close agreement across densities (standard deviation below 0.2 µm) confirms that this is supported by the data. The high-density lupine sample (Section 5) is anomalous and is excluded from the a_{eff} average. The fitted coefficients c_1, c_2 and b_1, b_2 are then optimised with a_{eff} fixed.

The resulting a_{eff} (2.96 µm for reed, 2.85 µm for lupine) is roughly three times smaller than the geometric fibre radius (8.95 µm and 10.6 µm), consistent with viscous

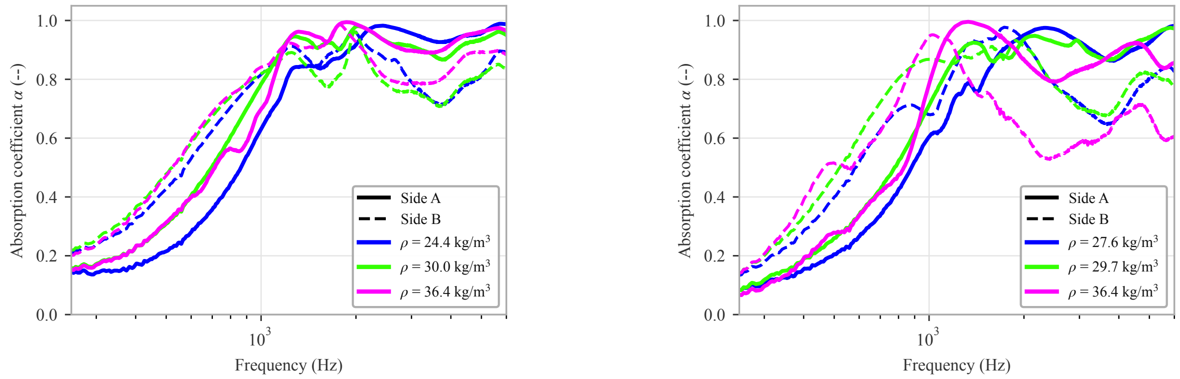

(a) Reed: measured absorption at three densities.

(b) Lupine: measured absorption at three densities.

Figure 2: Measured normal-incidence sound absorption coefficients for (a) reed and (b) lupine at three bulk density levels. Solid lines: Side A (open surface facing the source). Dashed lines: Side B (drainage mesh surface facing the source).

losses being governed by narrow inter-fibre constrictions rather than individual fibre surfaces. As the radius and the fixed literature coefficients are partially degenerate, a_{eff} should be regarded as a model-effective parameter rather than a direct measure of fibre geometry.

4. JCAL Parameter Identification

JCAL parameters were obtained using the RokCell software from the three-microphone impedance tube data, which provide the dynamic density $\tilde{\rho}(\omega)$ and dynamic bulk modulus $\tilde{K}(\omega)$ of the samples in addition to the absorption coefficient [8]. Rather than fitting the absorption coefficient alone, each parameter was adjusted against the measured quantity most sensitive to it: flow resistivity and tortuosity primarily against the dynamic density, and the thermal parameters against the dynamic bulk modulus, with the resulting computed absorption curve verified against the measured absorption curve as a final consistency check. Porosity was fixed to its computed value; airflow resistivity, tortuosity, and the characteristic lengths were adjusted freely.

Characterisation was performed separately for Side A and Side B, and for all measured samples (four per density). The two sides are treated as acoustically distinct configurations of the same material, not as two independent materials. Any difference in characterised parameters between the sides is therefore a consequence of the density gradient, not a material difference; this is a central distinction for the interpretation of the results.

5. Results and Discussion

5.1. Measured Sound Absorption and Orientation Dependence

Figure 2 shows the measured average absorption for reed and lupine foams at three density levels. The orientation dependence is immediately visible: Side A and Side B produce substantially different absorption curves across the full frequency range. Above approximately 1000 Hz, Side A achieves higher absorption; below this frequency, Side B absorbs more strongly. This crossover is a direct signature of the dense drainage layer: when it faces the rigid backing (Side A measurement), it acts as a high-resistivity termination that shifts the first absorption peak to lower frequencies while leaving the bulk network accessible to the incident wave. When it faces the source (Side B measurement), it acts as a high-impedance front face that improves low-frequency impedance matching but reduces broadband absorption.

This orientation dependence demonstrates that the acoustic response of these materials is governed not only by bulk properties but also by the spatial distribution of microstructural features relative to the boundary conditions. A homogeneous model cannot reproduce both orientations simultaneously with a single parameter set.

5.2. JCAL and Analytical Model Predictions

Figure 3 compares measured absorption with JCAL and analytical model predictions for both sides and materials. The JCAL model, fitted separately for each side, reproduces Side A accurately across the full frequency range for both materials and all density levels. For Side B, the fit is systematically worse, particularly in the mid-frequency range where the homogeneous model cannot capture the two-layer interaction. This confirms that Side B JCAL parameters are configuration-dependent effective quantities, not intrinsic material properties.

The analytical model, using an a_{eff} derived from Side A characterisation, captures the general trend of the Side A absorption for both materials, with systematic deviations in the frequency of the first absorption maximum that reflect the known limitations of idealised parallel-fibre models for disordered foam networks. For Side B the agreement is more variable: it remains good for reed but degrades for lupine, con-

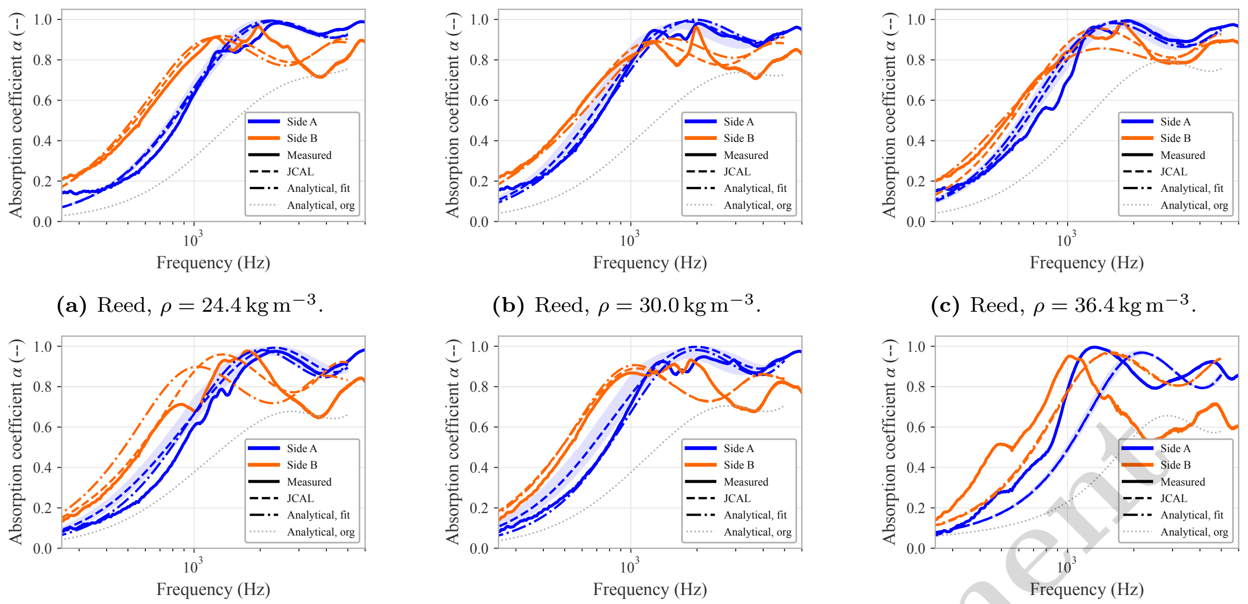

(a) Reed, $\rho = 24.4\,\mathrm{kg\,m^{-3}}$. **(b)** Reed, $\rho = 30.0\,\mathrm{kg\,m^{-3}}$. **(c)** Reed, $\rho = 36.4\,\mathrm{kg\,m^{-3}}$.

(d) Lupine, $\rho = 27.6\,\mathrm{kg\,m^{-3}}$. **(e)** Lupine, $\rho = 29.7\,\mathrm{kg\,m^{-3}}$. **(f)** Lupine, $\rho = 36.4\,\mathrm{kg\,m^{-3}}$.

Figure 3: Measured absorption compared with JCAL and analytical model predictions for reed (a–c) and lupine (d–f).

sistent with the model being parameterised from the bulk-representative Side A rather than the drainage-facing orientation. The high-density lupine sample (Figure 3f) is a clear outlier in both orientations, as expected for the anomalous measurement discussed in Section 5.

5.3. Non-Acoustic Parameters and Reliability of Flow Resistivity Measurements

Table 1 summarises the JCAL-characterised parameters for both sides and materials. Figure 4 shows the airflow resistivity and viscous characteristic length as a function of bulk density.

The most striking feature of the resistivity plots is the position of the whole-sample measured flow resistivity (gray squares): it sits substantially above both Side A and Side B JCAL-characterised values for all samples. This is a direct consequence of the ISO 9053 measurement integrating over the full sample thickness in series, so that the thin, high-resistivity drainage layer dominates the result and renders it unrepresentative of the bulk material. Standard whole-sample flow resistivity measurements are therefore unreliable as model inputs for inhomogeneous foam-formed materials.

The JCAL-characterised Side B resistivity is consistently higher than Side A, as expected since the dense layer is part of the acoustic path when Side B faces the source; the Side B value is an effective average that absorbs the influence of the gradient rather than a physical layer property.

For both reed (Figure 4a) and lupine (Figure 4c), the fitted analytical model reproduces the magnitude and overall density trend of the Side A characterised resistivity, with the fitted A curve passing close to the characterised points. Residual deviations remain, larger for lupine, indicating that the fibre packing geometry of these foam-formed materials departs from the idealised parallel-fibre assumption underlying the Tamayol relation [9].

The high-density lupine sample ($\rho = 36.4\,\mathrm{kg\,m^{-3}}$) yields an anomalously low characterised resistivity of approximately $10\,000\,\mathrm{N\,s\,m^{-4}}$ and a correspondingly high k_0' (Table 1), with a poor fit (Figure 3f). This is likely due to sample leakage or an unconverged inversion; the sample is excluded from the effective-radius determination in Section 3.

For the viscous characteristic length (Figures 4b and 4d), characterised values for both sides are significantly smaller than analytical predictions and show only weak density dependence. This is consistent with the softwood results [4] and indicates that viscous losses are controlled by micro-scale constrictions at fibre intersections rather than average pore size [12]. Side B values are systematically lower than Side A, reflecting the narrower pore geometry of the dense drainage layer.

6. Discussion

The central finding of this study is that homogeneous JCAL characterisation of foam-formed plant fibre materials produces configuration-dependent parameters rather than intrinsic material properties. The JCAL model fitted to Side B data absorbs the influence of the dense drainage layer into its parameter set, producing values – in particular a lower viscous characteristic length and higher flow resistivity – that differ systematically from Side A and cannot be attributed to the fibre network alone. Characterising only Side B would lead to parameters that are accurate for that specific orientation but misleading as material descriptors.

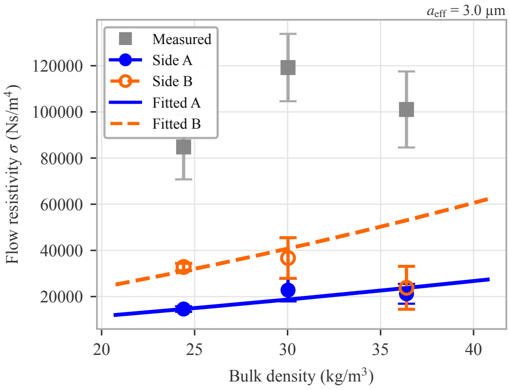

(a) Reed: airflow resistivity vs. density.

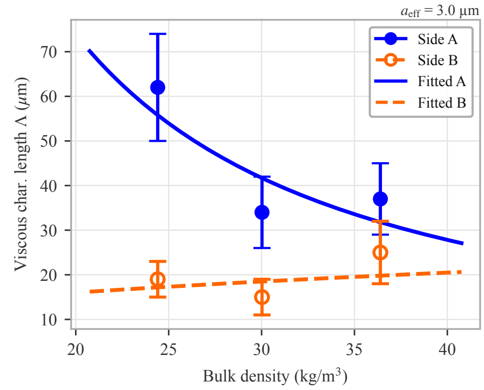

(b) Reed: viscous characteristic length vs. density.

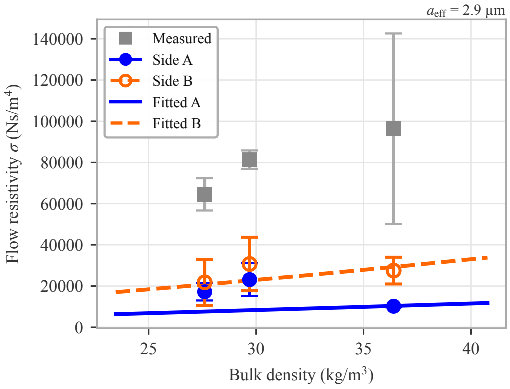

(c) Lupine: airflow resistivity vs. density.

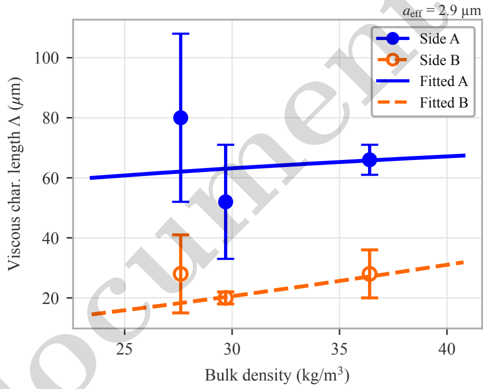

(d) Lupine: viscous characteristic length vs. density.

Figure 4: Airflow resistivity (a,c) and viscous characteristic length (b,d) vs. bulk density for reed (top) and lupine (bottom). Blue filled circles: Side A characterised (±std). Orange open circles: Side B characterised (±std). Gray squares: whole-sample measured flow resistivity (resistivity panels only) dominated by the dense drainage layer. Lines: fitted analytical model (blue solid: Side A; orange dashed: Side B); panel title gives a_{eff}.

This configuration-dependence also propagates into the analytical model. The effective fibre radius a_{eff} derived from Side A characterisation is physically interpretable as a property of the fibre network. An equivalent derivation from Side B would yield a smaller, biased estimate that reflects the dense layer rather than the fibres.

The whole-sample ISO 9053 flow resistivity measurement compounds this problem by providing a value that is even further from the bulk network properties than the Side B JCAL estimate. In series flow through a layered material, resistivity is dominated by the highest-resistivity layer regardless of its thickness fraction. This makes standard flow resistivity measurements fundamentally unreliable for inhomogeneous foam-formed materials, and underlines the importance of using JCAL-characterised Side A values as the basis for analytical model inputs.

The path forward is a layered transfer-matrix model in which the dense drainage layer and the bulk foam are characterised and modelled separately. The Side A and Side B JCAL parameters established in this study provide the layer-level inputs for such a model, and the density gradient directly observable from tomography [3] provides the physical basis for defining layer geometry without additional fitting.

7. Conclusions

This study investigated foam-formed reed and lupine fibre absorbers using impedance tube measurements from both the open surface (Side A) and the drainage mesh surface (Side B), and demonstrated three principal findings.

First, the acoustic absorption response depends strongly on sample orientation, with Side A and Side B producing substantially different curves across the full frequency range. This orientation dependence is a direct consequence of the density gradient inherent to the foam-forming process and cannot be reproduced by a homogeneous model.

Second, JCAL parameters obtained from inverse characterisation are configuration-dependent. Side B parameters are biased by the dense drainage layer and do not represent intrinsic material properties. Side A characterisation, where the bulk fibre network is the primary acoustic medium, provides the more physically meaningful basis for material characterisation and analytical model input.

Table 1: JCAL non-acoustic parameters obtained from inverse characterisation for foam-formed reed and lupine samples, separately for Side A and Side B. Values in parentheses indicate standard deviations.

Material	Side	ρ	σ	ϕ	α_∞	Λ	Λ'	k_0'
		$(\mathrm{kg\,m^{-3}})$	$(\mathrm{N s\,m^{-4}})$	(–)	(–)	(μm)	(μm)	$(10^{-10}\,\mathrm{m}^2)$
Reed	A	24.4	14600 (1200)	0.98	1.11 (0.06)	62 (12)	301 (93)	14 (2)
		30.0	22800 (4900)	0.98	1.13 (0.10)	34 (8)	312 (22)	21 (6)
		36.4	21200 (4300)	0.98	1.24 (0.09)	37 (8)	221 (45)	20 (8)
	B	24.4	32800 (1600)	0.98	1.20 (0.09)	19 (4)	350 (0)	61 (11)
		30.0	36700 (8800)	0.98	1.08 (0.09)	15 (4)	356 (12)	68 (17)
		36.4	23800 (9300)	0.98	1.32 (0.19)	25 (7)	671 (141)	35 (3)
Lupine	A	27.6	17200 (4200)	0.99	1.30 (0.19)	80 (28)	209 (87)	24 (7)
		29.7	23100 (8000)	0.99	1.30 (0.26)	52 (19)	176 (60)	20 (9)
		36.4	10200 (500)	0.98	1.31 (0.03)	66 (5)	380 (75)	295 (41)
	B	27.6	21800 (11200)	0.98	1.54 (0.28)	28 (13)	446 (108)	68 (29)
		29.7	30700 (13000)	0.98	1.62 (0.13)	20 (2)	302 (96)	64 (18)
		36.4	27500 (6500)	0.98	1.30 (0.01)	28 (8)	443 (154)	344 (143)

Third, whole-sample flow resistivity measurements following ISO 9053 are dominated by the thin, high-resistivity drainage layer and substantially overestimate the bulk resistivity. They should not be used directly as model inputs for inhomogeneous foam-formed materials.
Future work will extend this study to a layered transfer-matrix model using the Side A and Side B JCAL parameters as layer-level inputs, informed by tomography-derived density profiles [3].

References

[1] J. P. Arenas, R. del Rey, J. Alba, and R. Oltra, "Sound-absorption properties of materials made of esparto grass fibers," *Sustainability*, vol. 12, p. 5533, 2020. DOI: 10.3390/su12145533.

[2] T. Pöhler, P. Jetsu, and H. Isomoisio, "Benchmarking new wood fibre–based sound absorbing material made with a foam-forming technique," *Build. Acoust.*, vol. 23, no. 3-4, pp. 131–143, 2016. DOI: 10.1177/1351010X16661564.

[3] M. Langhans et al., "Foam-Formed Lupine and Reed Pulp: Anisotropic Bio-Based Foams for Sound Absorption Applications," *ACS Sustain. Resour. Manag.*, 2026, Preprint submitted May 2026.

[4] J. Heldmann, J. Cucharero, and T. Lokki, "Sound absorption of foam-formed softwood fibers: Characterization, modeling, prediction," *Appl. Acoust.*, vol. 245, p. 111 200, 2026. DOI: https://doi.org/10.1016/j.apacoust.2025.111200.

[5] J. Cucharero, S. Ceccherini, T. Maloney, T. Lokki, and T. Hänninen, "Sound absorption properties of wood-based pulp fibre foams," *Cellulose*, vol. 28, pp. 4267–4279, 2021. DOI: 10.1007/s10570-021-03774-1.

[6] L. Jaouen, E. Gourdon, and P. Glé, "Estimation of all six parameters of Johnson-Champoux-Allard-Lafarge model for acoustical porous materials from impedance tube measurements," *J. Acoust. Soc. Am.*, vol. 148, no. 4, pp. 1998–2005, 2020. DOI: 10.1121/10.0002162.

[7] T. Iwase, Y. Izumi, and R. Kawabata, "A new measuring method for sound propagation constant by using sound tube without any air spaces back of a test material," in *INTER-NOISE and NOISE-CON Congress and Conference Proceedings*, 1998, pp. 1265–1268.

[8] Y. Salissou and R. Panneton, "Wideband characterization of the complex wave number and characteristic impedance of sound absorbers," *J. Acoust. Soc. Am.*, vol. 128, no. 5, pp. 2868–2876, 2010.

[9] A. Tamayol and M. Bahrami, "Transverse permeability of fibrous porous media," *Phys. Rev. E*, vol. 83, no. 4, p. 046 314, 2011. DOI: 10.1103/PhysRevE.83.046314.

[10] F. Pompoli, "Acoustical characterization and modeling of sustainable posidonia fibers," *Appl. Sci.*, vol. 13, no. 7, p. 4562, 2023. DOI: 10.3390/app13074562.

[11] J. F. Allard and N. Atalla, *Propagation of sound in porous media*, 2nd. Chichester, UK: John Wiley & Sons, 2009. DOI: 10.1002/9780470747339.fmatter.

[12] O. Umnova, D. Tsiklauri, and R. Venegas, "Effect of boundary slip on the acoustical properties of microfibrous materials," *J. Acoust. Soc. Am.*, vol. 126, no. 4, pp. 1850–1861, 2009. DOI: 10.1121/1.3204087.